Journal of Molecular and Cellular Cardiology 156 (2021) 45–56

Contents lists available at ScienceDirect

Journal of Molecular and Cellular Cardiology

journal homepage: www.elsevier.com/locate/yjmcc

Creld1 regulates myocardial development and function

Vera Beckert [a,1], Sebastian Rassmann [a,1], Amir Hossein Kayvanjoo [b], Christina Klausen [a], Lorenzo Bonaguro [c], Dominik Simon Botermann [a,2], Melanie Krause [a,3], Kristin Moreth [d], Nadine Spielmann [d], Patricia da Silva-Buttkus [d], Helmut Fuchs [d], Valerie Gailus-Durner [d], Martin Hrabě de Angelis [d,e,f], Kristian Händler [g], Thomas Ulas [c,g], Anna C. Aschenbrenner [c,h], Elvira Mass [b,*,1], Dagmar Wachten [a,**,1]

[a] Institute of Innate Immunity, Biophysical Imaging, Medical Faculty, University of Bonn, 53127 Bonn, Germany
[b] Life & Medical Institute (LIMES), Developmental Biology of the Immune System, University of Bonn, 53115 Bonn, Germany
[c] Life & Medical Institute (LIMES), Genomics and Immunoregulation, University of Bonn, 53115 Bonn, Germany
[d] German Mouse Clinic, Institute of Experimental Genetics, Helmholtz Center Munich, German Research Center for Environmental Health, 85764 Neuherberg, Germany
[e] Chair of Experimental Genetics, School of Life Science Weihenstephan, Technical University Munich, 85354 Freising, Germany
[f] German Center for Diabetes Research (DZD), 85764 Neuherberg, Germany
[g] German Center for Neurodegenerative Diseases (DZNE), PRECISE Platform for Single Cell Genomics and Epigenomics at the DZNE and the University of Bonn, 53127 Bonn, Germany
[h] Department of Internal Medicine and Radboud Center for Infectious Diseases (RCI), Radboud University Medical Center, 6500HB Nijmegen, the Netherlands

ARTICLE INFO

Keywords:
Heart development
Creld1
Trabeculation
ECM
Notch

ABSTRACT

CRELD1 (Cysteine-Rich with EGF-Like Domains 1) is a risk gene for non-syndromic atrioventricular septal defects in human patients. In a mouse model, Creld1 has been shown to be essential for heart development, particularly in septum and valve formation. However, due to the embryonic lethality of global *Creld1* knockout (KO) mice, its cell type-specific function during peri- and postnatal stages remains unknown.

Here, we generated conditional Creld1 KO mice lacking Creld1 either in the endocardium (KO^{Tie2}) or the myocardium (KO^{MyHC}). Using a combination of cardiac phenotyping, histology, immunohistochemistry, RNA-sequencing, and flow cytometry, we demonstrate that Creld1 function in the endocardium is dispensable for heart development. Lack of myocardial Creld1 causes extracellular matrix remodeling and trabeculation defects by modulation of the Notch1 signaling pathway. Hence, KO^{MyHC} mice die early postnatally due to myocardial hypoplasia.

Our results reveal that Creld1 not only controls the formation of septa and valves at an early stage during heart development, but also cardiac maturation and function at a later stage. These findings underline the central role of Creld1 in mammalian heart development and function.

1. Introduction

AVSD is a common congenital heart malformation, which results from the failure of cardiac remodeling during the formation of the atrioventricular septa and valves. AVSD constitutes more than 7% of all recognized heart defects, and AVSD patients have to undergo surgical treatment in the first months after birth to prevent heart failure [1]. *CRELD1* has been the first single gene linked to atrioventricular septal defects (AVSD) [1]. Missense mutations were found in non-syndromic patients and in Down syndrome patients with AVSD [1–7].

To address the molecular function of Creld1 and how this protein could contribute to AVSD, we and others have analyzed the heart development in Creld1 knockout mice [8,9]. These studies reveal that Creld1 controls the formation of the atrioventricular cushion (AVC), the

* Corresponding author.
** Corresponding author at: Institute of Innate Immunity, Biophysical Imaging, University Hospital Bonn, University of Bonn, 53127 Bonn, Germany.
E-mail addresses: emass@uni-bonn.de (E. Mass), dwachten@uni-bonn.de (D. Wachten).
[1] Equally contributed.
[2] Current affiliation of D.S.B.: Institute of Cardiovascular Physiology, University Medical Center Göttingen, Göttingen, Germany.
[3] Current affiliation of M.K.: European Molecular Biology Laboratory (EMBL), Genome Biology Unit, Heidelberg, Germany.

https://doi.org/10.1016/j.yjmcc.2021.03.008
Received 5 December 2020; Received in revised form 25 February 2021; Accepted 18 March 2021
Available online 24 March 2021

progenitor structure of the developing septa, resulting in embryonic death at developmental day (E)11.5 due to a defect in heart development. AVC morphogenesis in mice occurs between E9.5 and E10.5. At this time point, endocardial cells within the heart tube start delaminating and subsequently invade the extracellular matrix (ECM), where they acquire mesenchymal properties and start to proliferate. This process - termed endocardial-mesenchymal transformation (EMT) - requires intricate interactions between the endocardium and the

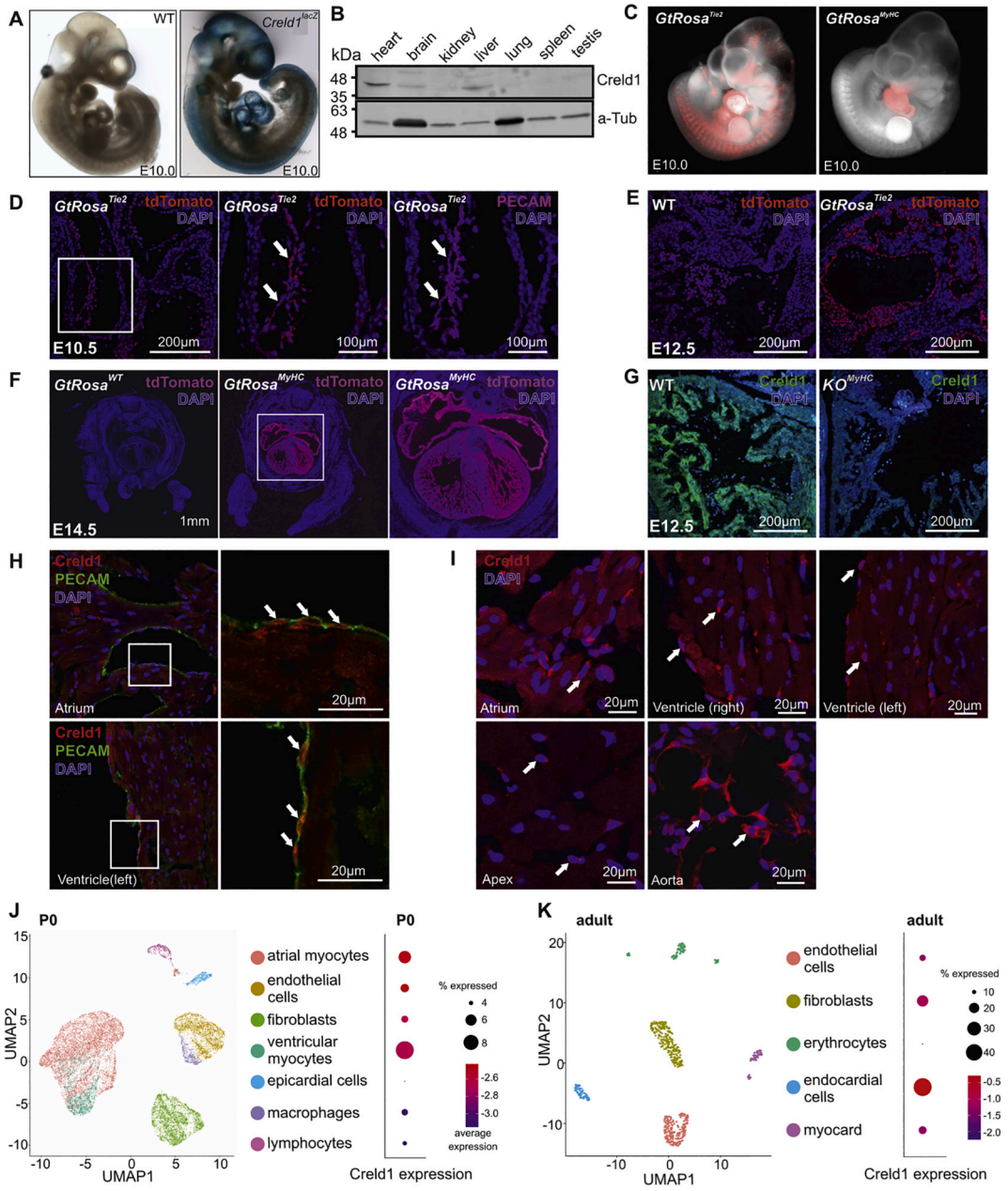

Fig. 1. Conditional Creld1 knockout mouse lines. (A) Whole-mount lacZ staining of WT and Creld1^{lacZ} embryos at E10.0. (B) Fluorescence of the tdTomato reporter (red) driven by either the Tie2- or the MyHC-Cre mouse line in non-fixed embryos at E10.5. DNA has been labeled using DAPI (blue). (C) Immunofluorescence staining against tdTomato (red), driven by the Tie2 promotor (GtRosa^{Tie2}, left), and PECAM (right, purple) in paraffin sections of E10.5 embryos. Only the region of the heart is shown; box indicates the atrioventricular (AV) cushion, which is shown in the magnified view in the middle; arrows indicate endothelial cells lining the heart lumen. (D) Immunofluorescence staining against tdTomato (red) in wild-type (WT) and transgenic E12.5 embryos expressing tdTomato driven by the Tie2 promotor (GtRosa^{Tie2}). (E) Immunofluorescence staining against tdTomato (red) in paraffin sections of E14.5 wild-type and transgenic embryos expressing tdTomato under the control of the MyHC promotor (GtRosa^{MyHC}). The right panel shows a magnification of the heart region indicated with a box in the middle panel. (F) Immunofluorescence staining against Creld1 (cyan) in paraffin sections of E12.5 wild-type (WT) and conditional KO^{MyHC} embryos at E12.5. (G) Western blot analysis of Creld1 protein expression in different tissues of an adult wild-type mouse. Alpha-Tubulin (α-Tub) has been used to verify that protein has been loaded. The protein marker (in kDa) is indicated. (H) Immunofluorescence staining against Creld1 (red) and PECAM (green) in cryo-section of the atrium and ventricle of an adult wild-type mouse. Boxes on the left indicate the region of the magnified view shown on the right; arrows highlight endothelial cells. (I) Immunofluorescence staining against Creld1 (red) in cryo-sections of different regions of an adult wild-type mouse heart (atrium, ventricle, apex, aorta). Scale bars are indicated. All images are representatives of at least $n = 3$ per genotype. (J) Cell clusters from single cell RNA-seq analysis of cardiac cells at postnatal day 0 (P0) visualized by UMAP. Cell types are color coded. The expression of *Creld1* in each cell type is visualized via dot plot. (K) Same as in (J) for adult cardiac cells. (For interpretation of the references to color in this figure legend, the reader is referred to the web version of this article.)

underlying myocardium [10,11]. Creld1 is required for the vascular endothelial growth factor (VEGF)-dependent proliferation of endocardial cells at E10.5 by promoting calcineurin-dependent nuclear translocation of nuclear factor of activated T cells 1 (NFATc1) and, thereby, the expression of Nfatc1 target genes [8]. After AVC formation is completed, the heart is further remodeled into the cardiac septa and valves. Creld1 is expressed in both endo- and myocardium [8]. However, Nfatc1 translocation only occurs in endocardial cells, which raises the question whether Creld1 predominantly functions in the endocardium. Besides cushion formation, the interaction between the endo- and myocardium also regulates the development and maturation of the ventricular wall and, thereby, formation of the mature heart. During development, the ventricular wall consists of the outer wall and the so-called trabeculae, which comprise myocardial cells covered by an endocardial cell layer. The compact ventricular wall mainly forms by proliferation of the outer cell layer. Loss of compaction leads to severe cardiac defects and eventually heart failure [12,13]. One of the major molecular players in regulating trabeculation is the Notch signaling pathway [14–17]. Whether Creld1 plays a role in regulating later stages of myocardial development, in particular after E11.5, is not known.

To unravel the cell type-specific function of Creld1 during heart development, we generated conditional knockout mice lacking Creld1 in either the endocardium or myocardium. Our results revealed that loss of Creld1 function in the endocardium is dispensable for heart development, whereas Creld1 function in the myocardium is essential for heart function and survival. In the myocardium, Creld1 controls modelling of the extracellular matrix (ECM) and trabeculation, and its loss resulted in myocardial hypoplasia. In turn, mice lacking Creld1 in the myocardium died shortly after birth. Our results reveal that Creld1 not only controls the formation of septa and valves at an early stage during heart development, but also maturation and function of the myocardium at a later stage. These findings underline the central role of Creld1 in mammalian heart development and function.

2. Results

2.1. Generation of conditional Creld1 knockout mice

Using global Creld1 knockout mice, we have previously shown that Creld1 controls cardiac development through activation of calcineurin/NFATc1 signaling [8]. However, Creld1 is widely expressed throughout the embryo and in adult tissues (Fig. 1A, B) [18]. Cardiac development crucially relies on signaling in both the endocardium and the myocardium. To unravel the cell type-specific contribution of Creld1 function during heart development, we generated conditional knockout (KO) mice lacking Creld1 in either the myocardium (KO^{MyHC}) or the endocardium (KO^{Tie2}). All investigations concerning mouse work have (i) local approval and (ii) all procedures conform to the guidelines from Directive 2010/63/EU of the European Parliament on the protection of animals used for scientific purposes (see Material and Methods part for details). Animals have been euthanized using isoflurane inhalation and cervical dislocation. We confirmed the specificity of the Cre lines using a tdTomato reporter line (GtRosa), analyzing the reporter fluorescence in the whole embryo (Fig. 1C) and on sections from embryos at different developmental stages (Fig. 1D–F). Expression of tdTomato in Tie2-Cre and MyHC-Cre mouse lines showed specific expression of the reporter transgene in endothelial cells or cardiomyocytes, respectively. The specificity of the MyHC-Cre line was further confirmed by lack of Creld1 expression in KO^{MyHC} cardiomyocytes (Fig. 1G). In the heart, Creld1 is expressed in endothelial cells, visualized by performing a co-staining with an antibody against the endothelial cell marker PECAM (Fig. 1H), but is also detected in the rest of the heart (Fig. 1I). To analyze Creld1 expression on a single-cell level in the heart at different developmental stages, we made use of already published single-cell RNA-seq data sets for the mouse heart at P0 and in the adult stage [19,20]. At P0, Creld1 is mainly expressed in atrial and ventricular myocytes, endothelial cells, and fibroblasts, and to a lesser extent in epicardial cells, and immune cells (Fig. 1J). In the adult state, Creld1 is mainly expressed in endocardial cells, and to a lesser extent in endothelial cells, myocardium, fibroblasts, and erythrocytes (Fig. 1K).

Of note, to verify the design of the conditional mouse line, we also generated global knockout mice by crossing $Creld1^{flox/flox}$ mice with Cre deleter mice [21]. In line with our previous report [8], viable wild-type, heterozygous, and homozygous embryos were identified at E10.0–10.5 at Mendelian ratios (wild-type: 27%, heterozygous: 49%, homozygous: 24%), but died soon after, and we never recovered any viable homozygous knockout mice after E11.5. Thus, we have generated conditional KO mice that allow studying Creld1 function specifically in the endocardium and myocardium.

2.2. Creld1 function in the endocardium is dispensable for heart development and function

To generate KO^{Tie2} mice and control littermates, we crossed $Tie2^{+/cre}$; $Creld1^{flox/flox}$ males with $Tie2^{+/+}$; $Creld1^{flox/flox}$ females (Fig. 2A). KO^{Tie2} mice ($Tie2^{+/cre}$; $Creld1^{flox/flox}$) were born in Mendelian ratio and survived to adulthood without any gross phenotype. To investigate in detail whether the loss of Creld1 in the endocardium affects cardiac function in adult mice, we performed a detailed analysis using histology, ultrasound, and echocardiography. Morphological analysis of isolated hearts from KO^{Tie2} mice did not reveal any septum defects or other morphological changes compared to control mice (Fig. 2B). The left diastolic diameter of KO^{Tie2} mice was slightly reduced (Fig. 2C), whereas the length of the QRS interval was not different to control littermates (Fig. 2D). To also investigate the cardiac phenotype on a cellular level, we determined the average area per cell in hematoxylin/eosin-stained sections. However, we did not observe a significant difference in cell area between control and KO^{Tie2} mice (Fig. 2E). Of note, to verify the results from KO^{Tie2} mice, we also generated mice lacking Creld1 in Nfatc1-expressing cells (KO^{Nfatc1}). The expression of the Cre recombinase in this model seemed to be more widespread than in the Tie2 model, as demonstrated using the fluorescence reporter mice (Supplementary Fig. S1A). Nevertheless, the ratio of KO^{Nfatc1} mice at weaning (3 weeks of age) was similar to KO^{Tie2} mice (Supplementary Fig. S1A). Thus, KO^{Nfatc1} and KO^{Tie2} mice display a similar phenotype and do not show an overt cardiac phenotype, demonstrating that endocardial Creld1 is dispensable for heart development and function.

2.3. Creld1 function in the myocardium is essential for cardiac function and survival

During the generation of KO^{MyHC} mice, we never recovered KO^{MyHC} mice at weaning age, indicating that these mice die during embryonic development or before weaning. To elucidate the time point of KO^{MyHC} mice lethality, we analyzed the distribution of viable embryos at E10.5 and E13.5 with the respective genotypes from matings of $MyHC^{+/cre}$; $Creld1^{+/flox}$ males with $MyHC^{+/+}$; $Creld1^{flox/flox}$ females (Fig. 3A). KO^{MyHC} embryos ($MyHC^{+/cre}$; $Creld1^{flox/flox}$) were recovered at ratios that were similar to control littermates at both developmental stages (Fig. 3A), demonstrating that loss of Creld1 in the myocardium does not lead to embryonic death before E13.5 and, therefore, does not resemble the global Creld1 knockout phenotype. Thus, we analyzed the survival after birth, revealing that KO^{MyHC} pups die shortly after birth, with few animals surviving until P13 (Fig. 3B). Postnatal KO^{MyHC} mice were smaller than their littermate controls, as demonstrated by the difference in body weight across the different time points (Fig. 3C). To reveal whether KO^{MyHC} mice die due to cardiac defects, we analyzed the gross heart morphology between P0 and P7. Indeed, the atria of postnatal KO^{MyHC} mice were severely enlarged and the ventricles displayed myocardial hypoplasia (Fig. 3D), indicating that KO^{MyHC} mice die due to heart failure. To reveal when the phenotypic differences occur during development, we analyzed the gross heart morphology of E13.5

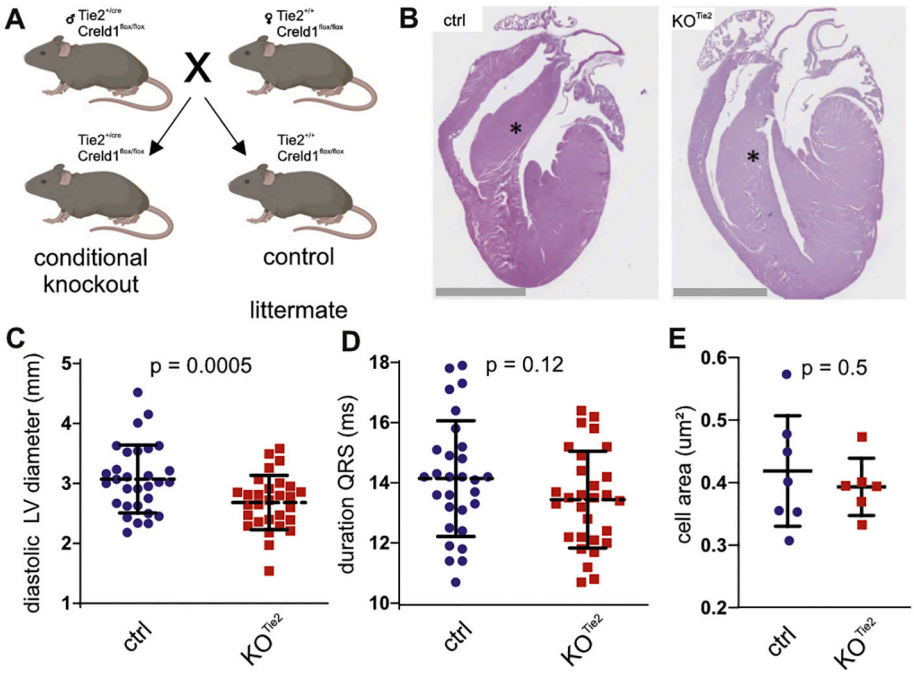

Fig. 2. Loss of Creld1 in the endocardium is not essential for cardiac function and survival. (A) Mating scheme for the generation of control and KO^{Tie2} mice. (B) Hematoxylin-eosin staining of cardiac sections from wild-type and KO^{Tie2} mice. Scale bar: 2.5 mm. Asterisk: interventricular septum. (C) Diastolic left ventricular diameter of wild-type ($Tie2^{+/+}$, $Creld1^{flox/flox}$, $n = 30$) and knockout mice ($Tie2^{+/cre}$, $Creld1^{flox/flox}$, $n = 29$). (D) see (C) for duration of the QRS interval. (E) Cell area. Data are shown as mean ± SD and individual data points. Statistical comparison has been performed using Student's *t*-test (two-tailed, unpaired, Welch correction). All images are representatives of at least n = 3 per genotype.

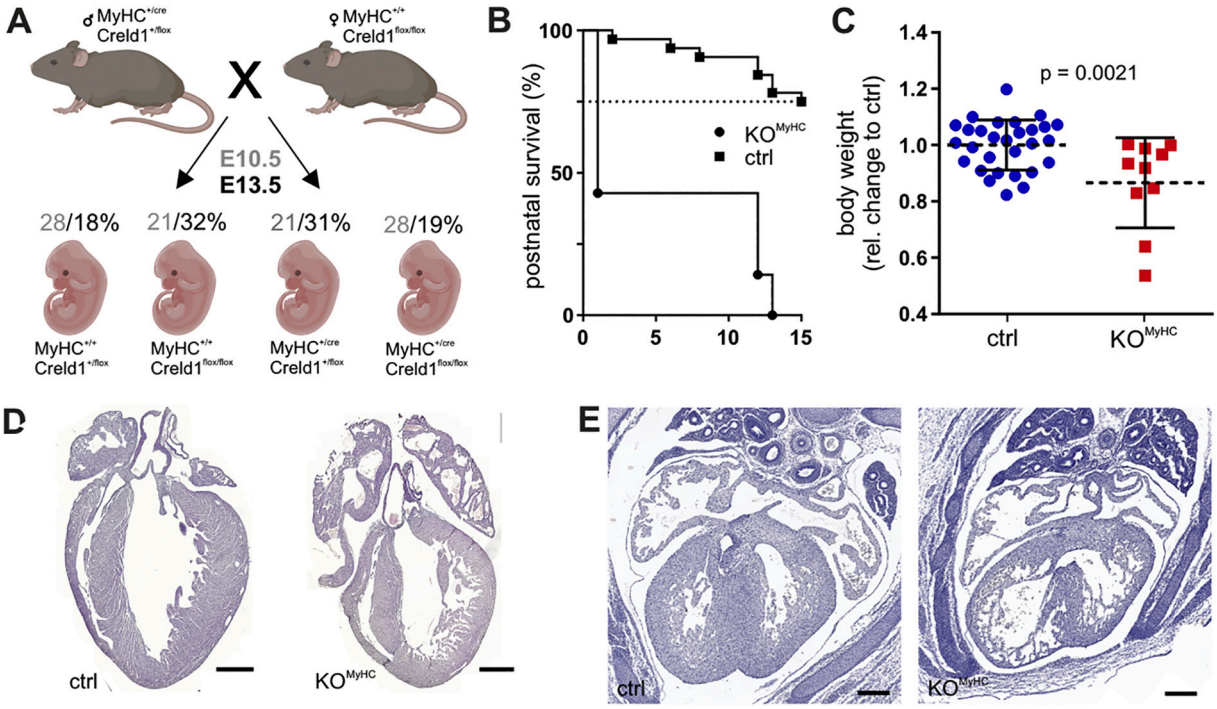

Fig. 3. Creld1 expression in the myocardium is essential for cardiac function and survival. (A) Mating scheme for the generation of control and KO^{MyHC} knockout mice. Percentages of genotypes at E10.5 (grey, $n = 53$) and E13.5 (black, $n = 138$) are indicated. (B) Survival rate of wild-type (ctrl) and KO^{MyHC} mice after birth. Days after birth are indicated. (C) Relative body weight of control (ctrl) and KO^{MyHC} mice. Weights have been determined from P0-P13 and normalized to the mean weight of the respective control littermates. Statistical comparison has been performed using Student's t-test (two tailed, unpaired). Data are shown as mean ± SD and individual data points. (D) Hematoxylin-eosin staining of cardiac sections from wild-type (ctrl) and KO^{MyHC} mice at P7. Similar results were obtained from other mice at P0 and P5. Scale bar: 0.4 mm. (E) Hematoxylin-eosin staining of cardiac sections from wild-type (ctrl) and KO^{MyHC} mice at E13.5. Scale bar: 0.2 mm. All images are representatives of at least n = 3 per genotype.

embryos. In fact, KO^{MyHC} embryos showed phenotypic differences compared to their control littermates: the cardiac wall of KO^{MyHC} embryos failed to mature properly with trabeculae being morphologically distinct and not yet compacting (Fig. 3E). Furthermore, E13.5 KO^{MyHC} embryos presented with an intra-ventricular shunt (IVS), whereas ventricles were already fully septated in wild-type littermates (Fig. 3E), indicating a delayed septation. In summary, the cardiac defects leading to postnatal death of KO^{MyHC} mice are already initiated during

embryonic development.

2.4. Myocardial Creld1 deficiency affects gene expression during heart development

To unravel the molecular mechanisms underlying dysmorphogenesis in the absence of Creld1 in the myocardium, we performed gene expression studies. So far, Creld1 function has only been associated with calcineurin/NFATc1 signaling at E10.5 during embryonic development in global Creld1 knockout mice [8]. However, the expression of NFATc1 target genes, *Nfatc1*, *Rcan1*, and *Vegfa* in KO^{MyHC} hearts was not significantly different at E10.5 compared to wild-type embryos (Supplementary Fig. S2A), indicating that the cardiac defects are not caused by dysregulation of NFATc1 signaling. To further delineate the underlying signaling pathways, we performed RNA sequencing (RNA-seq) of whole embryonic hearts at E13.5 and separated atria and ventricles at P3 (Fig. 4A). Dimensionality reduction using principal component analysis (PCA) of KO^{MyHC} samples and littermate controls revealed a clear separation of KO^{MyHC} samples and littermate controls by age and anatomy (Fig. 4B). While both genotypes clustered together at E13.5, P3 KO^{MyHC} and wild-type samples showed clear segregation according to genotype, indicating distinct transcriptomic profiles. To characterize signaling pathways that are co-expressed across all samples, we first performed a gene co-expression network analysis, based on the 'Construction of co-expression network – automated' (CoCena^2) [22] that clusters genes into distinct modules based on their expression patterns across genotypes and conditions. Similar to the PCA, we did not detect large differences between control and KO^{MyHC} E13.5 hearts (Fig. 4C). However, CoCena^2 identified the light green module with 310 genes globally upregulated in embryonic hearts and only the P3 KO^{MyHC} atria

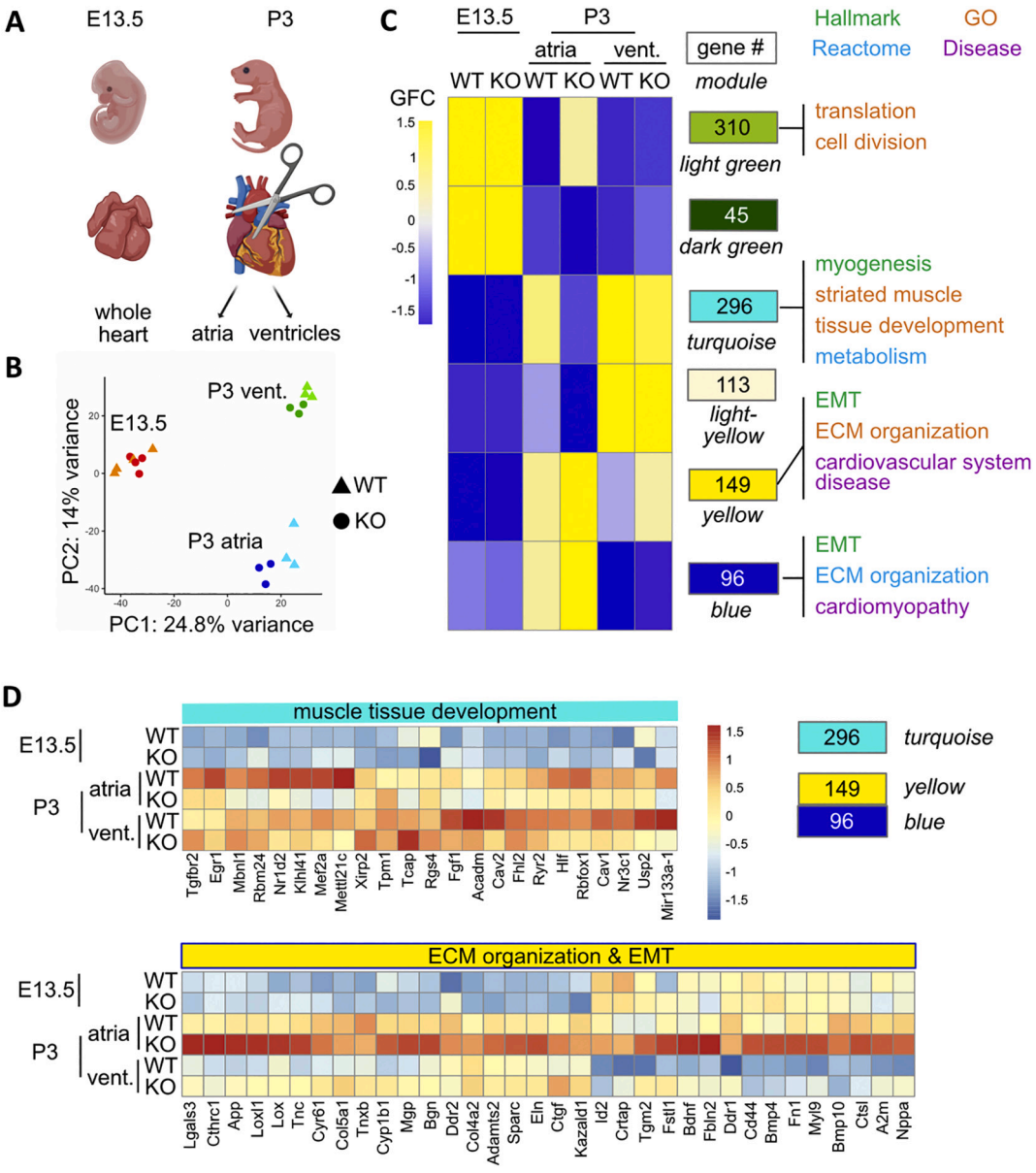

Fig. 4. Transcriptome analysis of control and KO^{MyHC} hearts. (A) Scheme of samples collected for RNA-seq. (B) Principal component analysis of E13.5 and P3 samples. (C) Genes were clustered into expression modules based on similar expression patterns across the experimental groups using a gene co-expression network analysis based on CoCena^2. Mean group fold change (GFC) for each module are displayed in the heat map. The number of genes assigned to specific modules are depicted in colored boxes on the right. (D) Heatmap representation of selected genes present in the turquoise, blue and yellow modules; ctrl: control hearts; KO KO^{MyHC} hearts. ECM: extracellular matrix, EMT: endocardial-mesenchymal transition. (For interpretation of the references to color in this figure legend, the reader is referred to the web version of this article.)

having a similar gene-expression signature (Fig. 4C). Gene ontology (GO) enrichment analysis of these genes suggested that embryonic hearts and P3 KO^{MyHC} atria are highly proliferative with the most prominent terms being 'translation' and 'cell division'. Further, P3 KO^{MyHC} atria showed decreased expression of genes important for muscle development, e.g. *Mef2a*, *Nr1d2*, and *Cav1,* when compared to control atria and ventricles (turquoise module, 296 genes, Fig. 4D). The yellow module (149 genes) contained genes that were upregulated in P3 KO^{MyHC} atria and ventricles and Hallmark and GO enrichment analyses revealed that these belong to biological processes of 'extracellular matrix (ECM) organization' and 'epithelial-to-mesenchymal transition (EMT)'. Similarly, the blue module (96 genes) identified 'ECM organization', 'EMT', and 'cardiomyopathy' using Reactome, Hallmark, and disease ontology analyses (Fig. 4C). These two modules contained collagens (*Col5a1*, *Col4a2*) and lysyl oxidases (*Lox*, *Loxl1*), suggesting an accumulation of ECM. Further, we detected increased expression of the natriuretic peptide progenitor A (*Nppa*) gene in both P3 KO^{MyHC} atria and ventricles. Nppa is the precursor of the Atrial natriuretic peptide (Anp) protein, which is secreted from cardiomyocytes upon stretching and dilation of the heart and, thus, serves as marker for mechanical stress as well as cardiac hypertrophy and heart failure [23]. Taken together, our analyses demonstrate that loss of myocardial Creld1 affects transcriptional networks in both atria and ventricles at P3.

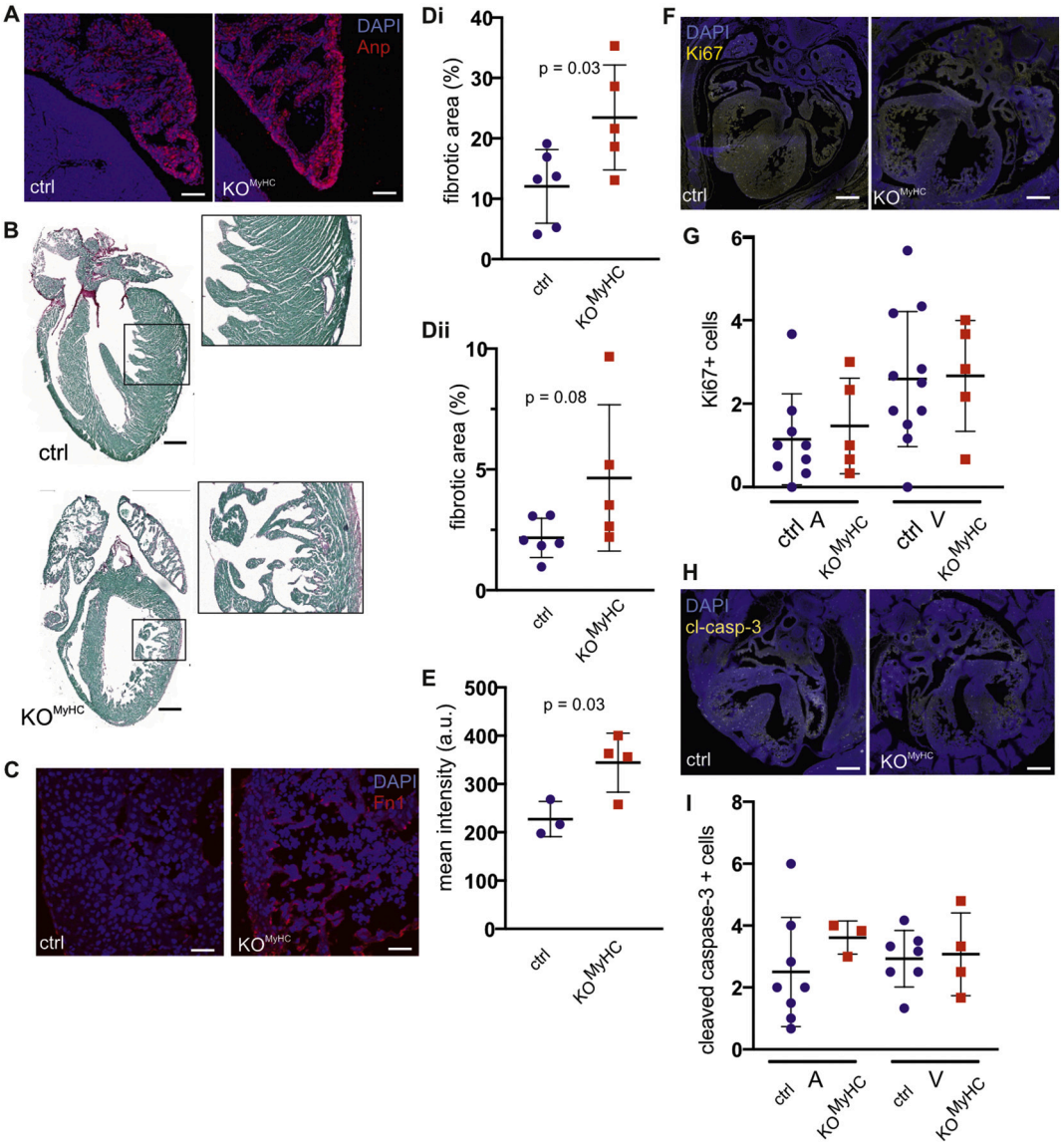

Fig. 5. Molecular and cellular cardiac phenotype of E13.5 KO^{MyHC} mice. (A) Anp (atrial natriuretic peptide) expression. Cardiac sections of P7 KO^{MyHC} and control mice labeled with an Anp antibody (red) and DAPI (blue). Scale bar: 120 μm. (B) Sirius Red/Fast Green labeling of cardiac sections from P7 KO^{MyHC} and control mice. Region indicated with a box is shown as a magnified view on the right. Similar results were obtained from other mice at P0 and P5. Scale bar: 0.4 mm. (C) Fn1 (Fibronectin 1) expression. Cardiac sections of E13.5 KO^{MyHC} and control embryos labeled with an Fn1 antibody (red) and DAPI (blue). Scale bar: 40 μm. All images are representatives of at least n = 3 per genotype. (D) Quantification of the fibrotic area: i. in the left atria, ii. in the left ventricles using images as shown in (B). (E) Quantification of the mean fluorescence intensity of the Fn1 labeling, as shown in (C). (F) Representative images of Ki67 labeling (yellow) of heart sections from E13.5 control and KO^{MyHC} mice. Dapi labeling is shown in blue. Scale bar: 250 μm. (G) Quantification of Ki67 labeling shown in (F). (H) Representative images of cleaved caspase-3 labeling (yellow) of heart sections from E13.5 control and KO^{MyHC} mice. Dapi labeling is shown in blue. Scale bar: 250 μm. (I) Quantification of cleaved caspase-3 labeling shown in (H). A: atria, V: ventricle. Statistical comparison has been performed using Student's t-test (two tailed, unpaired). Data are shown as mean ± SD and individual data points. (For interpretation of the references to color in this figure legend, the reader is referred to the web version of this article.)

2.5. Loss of Creld1 in the myocardium leads to ECM remodeling during heart development

To verify changes in gene expression identified by RNA-seq, we performed immunofluorescence labeling of Anp. Indeed, Anp expression was increased in the atria of KO^{MyHC} hearts (Fig. 5A). To histologically verify the accumulation of ECM, we performed Sirius Red/Fast Green staining for collagen detection. Whereas control hearts did not show prominent collagen deposition in the ventricular wall, KO^{MyHC} hearts displayed collagen accumulation surrounding the ventricular trabeculae (Fig. 5B), supporting a fibrotic phenotype in early postnatal KO^{MyHC} mice. In fact, the fibrotic area in both, atria and ventricles was significantly increased in KO^{MyHC} compared to control mice (Fig. 5D). During heart development, the ECM guides the assembly and maturation of cardiac cell types [24]. Mutations in the ECM genes *Has2* or *Vcan* prevent trabeculae formation [25,26], demonstrating the importance of the ECM for heart development and function. To investigate whether early changes in ECM during embryonic development might underlie the cardiac defects observed in KO^{MyHC} mice, we analyzed the ECM at E13.5 using Fibronectin 1 (Fn1) as a marker. Indeed, expression of Fn1 was increased in KO^{MyHC} compared to control hearts (Fig. 5C, E), demonstrating that ECM remodeling occurs already before major transcriptional changes can be observed. Apart from Fn1, also the expression of Laminin B3 was increased in KO^{MyHC} compared to control hearts (Supplementary Fig. S2C). To reveal whether a defect in proliferation underlies the defects observed at E13.5 in KO^{MyHC} hearts, we labeled heart sections with an antibody against Ki67. However, we did not observe any significant differences, neither in the atria, nor in the ventricles (Fig. 5F, G). In addition, we also did not observe increased cell death in KO^{MyHC} compared to control hearts (Fig. 5H, I). In summary, loss of Creld1 in the myocardium leads to ECM accumulation, resulting in myocardial hypoplasia and, eventually, heart failure.

2.6. Creld1 controls Notch1 signaling in the heart during embryonic development

To characterize Creld1-dependent signaling pathways during embryonic development that control ECM remodeling and trabeculation, we further inspected the gene expression at E13.5. Due to the major transcriptional changes at P3 and the settings used for analysis, the $CoCena^2$ analysis did not show any genes affected during embryogenesis. Thus, we generated a differentially expressed gene (DEG) list (*p*-value: <0.05) using only the E13.5 samples and performed a targeted gene-set enrichment analysis (GSEA) of cardiac development signaling pathways. However, neither genes with NFAT binding sites in their promoter, nor genes regulated by Vegf, Nrg1, or Bmp showed an unequivocal tendency towards being up- or down-regulated (Supplementary Fig. S3, Supplementary Table S2).

Intriguingly, screening of DEG between wild-type and KO^{MyHC} hearts at E13.5 revealed that Notch1, which is a well-known player during trabeculation and ECM degradation, is significantly downregulated in KO^{MyHC} compared to control hearts (p-value: 0.046, log2FC: -0.824). Notch1 signaling promotes ECM degradation during the formation of endocardial projections that are critical for trabeculation [17]. Some of the main components of Notch signaling controlling ECM remodeling and trabeculation are the E3 ligase Mib1, which ubiquitinates the Notch1 ligands Delta (Dll4) and Jagged (Jag1), triggering their endocytosis and initiating Notch1-dependent gene expression [27]. During early ventricular development, Dll4 is expressed in the endocardium, whereas Jag1 is expressed in the myocardium [14,15]. At E13.5, Notch1 activity depends on myocardial Jag1 expression, coordinating ventricular patterning and maturation [14,15]. Myocardial Jag1 inactivation disrupts chamber maturation, leading to cardiomyopathy [15]. First, we performed qPCR analysis on E13.5 hearts for Notch1 target genes (*Hey1*, *Hey2*, *Hes1*). However, we did not observe a difference in Notch1-dependent gene expression (Supplementary Fig. S1B). To analyze and spatially dissect Notch signaling in the *endo-* or myocardium, we performed flow cytometry analysis of E13.5 control and KO^{MyHC} hearts and analyzed the surface expression of Jag1. Generally, the frequency of endocardial ($CD31^+$) or myocardial ($Vcam1^+$) cells remained unchanged between control and KO^{MyHC} hearts (Supplementary Fig. S4A). To perform an unbiased analysis of Jag1 expression, we used Uniform Manifold Approximation and Projection (UMAP), a dimensional reduction technique to identify differences in endocardial and myocardial protein expression (Fig. 6A, Supplementary Fig. S4B). The analysis revealed no differences in the cluster distribution between control and KO^{MyHC} hearts (Fig. 6A). However, Jag1 expression, in particular in the $Vcam1^+$ clusters, was reduced in KO^{MyHC} hearts compared to control hearts (Fig. 6B). Gating-based flow cytometry analysis (Supplementary Fig. S4C) of Jag1 expression underlined these results (Fig. 6C). In summary, our results demonstrate that loss of Creld1 in the myocardium reduces Jag1 surface expression on myocardial cells at E13.5, which, in turn, alters Notch1 signaling and, thereby, heart development.

3. Discussion

Our study unravels the role of Creld1 in the embryonic and early postnatal heart and demonstrates that Creld1 function in the myocardium, but not the endocardium, is essential for heart function and survival. Together with results from our previous study [8], this suggests a key role for Creld1 in cardiac development with its functions being as diverse as the sequential molecular pathways necessary to form a four-chambered heart.

Based on Creld1 function in controlling AVC formation via activation of calcineurin/Nfatc1 signaling [8], we hypothesized that Creld1 exerts its role via a cell-autonomous mechanism in the endocardium. However, KO^{Tie2} mice, in which Creld1 is specifically depleted in the endocardium, did not cause a strong cardiac defect, demonstrating that endocardial Creld1 expression is dispensable for heart development and function. However, KO^{MyHC} mice lacking Creld1 in the myocardium died due to a severe cardiac defect a few days after birth. Thus, Creld1 function in the myocardium is essential for heart function and survival. Intriguingly, these mice did not resemble the phenotype of global Creld1 knockout-mice. Together, this indicates that the regulation of AVC development at E9.5–10.5 depends on Creld1 function in both, endocardium and myocardium. This points towards a role for Creld1 in controlling cell-cell communication between the myocardium and another cell type during early embryonic development. At later stages during development, the cell autonomous role of myocardial Creld1 seems to be more important. The molecular details underlying this Creld1-dependent interaction between different cell types in the heart need to be revealed in future studies. Of note, the other mammalian isoform, Creld2, is a secreted protein that fulfils paracrine functions [28,29]. Future studies need to reveal whether Creld1 also displays extracellular functions, promoting paracrine signaling.

Our gene expression analyses at P3 indicate that KO^{MyHC} atria show traits of the transcriptional program of E13.5 hearts. This is in line with previous studies showing that the remodeling process leading to a hypertrophic heart also includes a partial return to the expression of an embryonic gene program [30]. Our data further demonstrate that Creld1 expression in the myocardium promotes ECM remodeling, trabeculation, and chamber maturation. Loss of Creld1 resulted in an increased expression of ECM components at E13.5 (i.e. Fn1). The ECM provides the architectural scaffold to support efficient contraction and relaxation of cardiomyocytes and facilitates intercellular communication and metabolic exchange within the myocardial microenvironment [31]. Pathological ECM remodeling leads to adverse cardiac remodeling and heart failure [31]. In fact, increased Fn1 levels contribute to the development of cardiac hypertrophy [32] and persistent ECM and cardiomyocyte growth, as we observed in KO^{MyHC} hearts [17]. A key player in ECM remodeling, trabeculation, and chamber maturation is the Notch signaling pathway. A previous study showed that heterozygous $Creld1^{+/}$

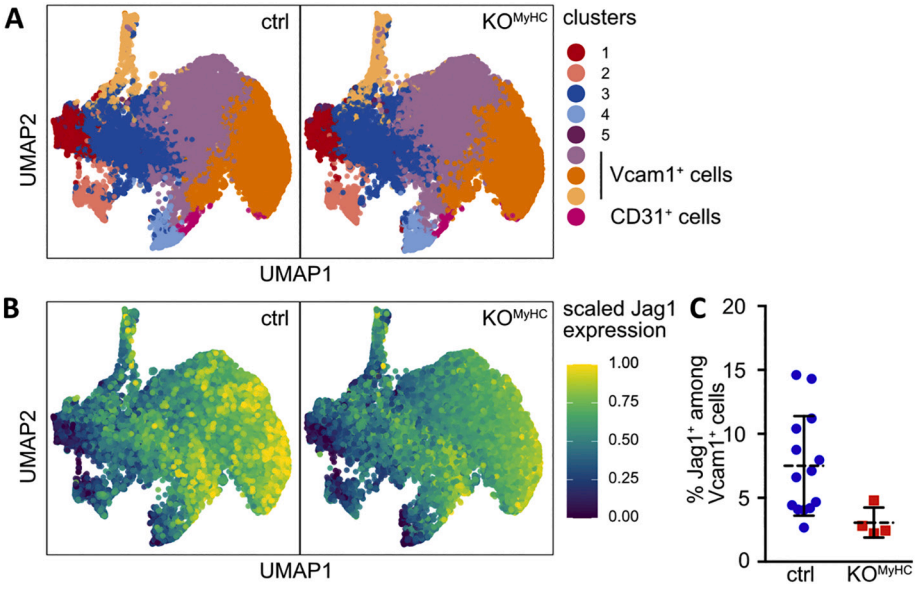

Fig. 6. Flow cytometry analysis of E13.5 hearts. (A) Clustering of CD45^{-}Ter119^{-} (immune cells, erythrocytes) cardiac cells. Individual clusters are color-coded; Vcam1^{+} and CD31^{+} are highlighted. ctrl: control hearts, KO^{MyHC}: knockout hearts. (B) Scaled Jag1 expression, superimposed on clustering presented in (A). All cluster presented in (A) and (B) are representative for $n = 4$ per genotype, 8 samples in total from 4 different experiments. (C) Percentage of Jag1^{+} cells among Vcam1^{+} cells. Data are presented as mean ± SD and individual data points.

$^{-}$ knockout mice display reduced expression of *Hey2* [33], which is a target of Notch1 signaling. In fact, also *Notch1* expression was reduced in Creld1$^{+/-}$ knockout mice [33]. Our results indicate that Creld1 in the myocardium controls Notch1 signaling by stimulating the surface expression of Jag1 in the myocardium, thereby enhancing trabecular termination, and contributes to compaction. However, loss of Jag1 in cardiomyocytes does only results in a mild cardiac phenotype without a defect in trabeculation [15], indicating that down-regulation of Jag1 alone does not underlie the cardiac defects observed in KO^{MyHC} hearts. Furthermore, it is surprising that loss of Creld1 in the myocardium only results in minor changes in gene expression during embryonic development, nevertheless, neonatal mice die soon after birth. This conundrum has to be solved in future experiments.

So far, Creld1 has been shown to interact with calcineurin B, which controls Nfatc1 translocation in the nucleus [8]. Furthermore, Creld1 regulates surface expression of the acetylcholine receptor (AChR) in mouse muscle cells by promoting the assembly of AChR subunits in the ER [34]. Thus, Creld1 seems to be important for regulating the subcellular localization of proteins. Whether this also plays a role in the context of Notch signaling in the myocardium will be investigated in future studies. Previous work indicated that the predicted structure of Creld1 is reminiscent of non-canonical Notch1 ligands, e.g. Dlk1 [35], lacking the DSL motif of canonical Notch ligands and rather containing tandem EGF repeats. However, physical interaction between Creld1 and Notch1 could not be verified [33].

A recent study, investigating the role of CRELD1 in the immune system, identified CRELD1 as an important modulator of immune homeostasis upstream of WNT signaling [18]. This suggests that WNT and Notch signaling are connected, as *Jag1*, which is down-regulated in hearts of myocardium-specific Creld1 KO animals, is a target gene of canonical WNT signaling [36–38].

Altogether, these results uncover a previously undescribed function for Creld1 signaling and demonstrate that Creld1 and Notch1 signaling are closely intertwined in the myocardium during heart development.

AVSD patients carrying *CRELD1* mutations globally express the mutation in both endocardium and myocardium. Thus, the patients display a defect in septum and valve formation due to defects in AVC formation. However, no defects in chamber maturation have been reported, which would be a result of CRELD1 loss-of-function in the myocardium. To mimic the human pathophysiology and further analyze the functional consequences of Creld1 mutations *in vivo*, knock-in mouse models carrying Creld1 mutations are required that express the mutant protein in a cell type-specific manner. Our study has added another chapter to understand the molecular mechanisms underlying cardiac development and underlines the key role of Creld1 in regulating cardiac development and heart function.

4. Material and methods

Mice. All investigations concerning mouse work have (i) local approval and (ii) all procedures conform to the guidelines from Directive 2010/63/EU of the European Parliament on the protection of animals used for scientific purposes. In detail, all animal experiments were conducted according to the German law of animal protection and in agreement with the approval of the local institutional animal care committees (caesar: Landesamt für Natur, Umwelt und Verbraucherschutz (LANUV), North Rhine-Westphalia, Az 84-02.04.2014. A275; German Mouse Clinic: district government of Upper Bavaria, Az ROB-55.2-2532.Vet_02-16-46). Animal housing, handling and procedures were performed according to the guidelines governing animal care. Mice were housed under standard SPF conditions (12-h light/dark cycle) with food and water provided ad libitum. Targeted ES cells (Creld1$^{tm1a(EUCOMM)Wtsi}$) were obtained from the European Mouse Mutant Cell Repository (EuMMCR) and injected into blastocysts (84-02.04.2012.A192) to generate Creld1^{lacZ} mice as described previously [8]. To remove the lacZ/neo cassette and generate the conditional allele (Creld1^{flox}), offspring was crossed to Flp-deleter mice [39]. To generate cell type-specific knockout mice, Creld1^{flox} mice were crossed with respective Cre lines: Tie2-Cre [40], Nfatc1-Cre [41], or αMyHC-Cre [42]. As a reporter, Gt(Rosa)26Sor$^{tm9(CAG-tdTomato)Hze}$ (GtRosa) mice were used [43]. Animals have been euthanized using isoflurane inhalation and cervical dislocation.

Genotyping. Genotyping was performed using isolated DNA obtained from ear punches. Primers for detecting the lacZ cassette of Creld1-lacZ mice were C2411 (5′ TGCAGTCGGGAATCTG) and C2413 (5′ AGTCTTCCTGTCCAGG); transgenic band 450 bp. Primers for detecting the floxed allele after removal of the lacZ cassette of Creld1flox mice were C2411 and C2412 (5′ TGGGCACACTTCTGTG); wild-type band 250 bp and transgenic band 320 bp. Primers for detecting the KO allele after removal of the floxed cassette mice were C2411 and C2414 (5′ TCAGGGACTGAACTCC); transgenic band 469 bp. Generic primers for detecting the Tie2-Cre or Nfatc1-Cre allele were C0098 (5′ GCGGTCTGGCAGTAAAAACTATC) and C0099 (5′ GTGAAA-CAGCATTGCTGTCACTT); transgenic band 180 bp. MyHC-Cre specific

primers were C3750 (5′ ATGACAGACAGATCCCTCCTATCTCC) and C3751 (5′ CTCATCACTCGTTGCATCGAC); transgenic band 300 bp.

X-Gal staining. Mouse embryos were fixed in 0.5% paraformaldehyde in PBS for 1 h at 4 °C, washed in PBS twice and incubated in rinse solution (100 mM NaP, 2 mM $MgCl_2$, 0.01% sodium deoxycholate, 0.02% NP-40) for 1 h. Afterwards, samples were stained for 24 or 48 h in X-gal staining solution (1 mg/ml X-gal, 5 mM K4[FeII(CN)6], 5 mM K3[FeIII(CN)6]), washed for 1 h in PBS and mounted using 100% glycerol.

Immuno- and histological stainings and quantification. Mouse embryos and hearts were fixed in 4% paraformaldehyde/PBS for 6 h (E10.5) or 48 h (E13.5, postnatal hearts). For cryo-sections (postnatal hearts), samples were cryo-protected in 10%/30% sucrose for 48 h, and embedded in Tissue Tek (Sakura Finetek). To block unspecific binding, cryo-sections (16 μm) were incubated for 1 h in blocking buffer (0.5% Triton × 100 and 5% ChemiBLOCKER (Millipore) in 0.1 M phosphate buffer, (pH 7.4)). Primary antibodies were diluted in blocking buffer and incubated for 2 h. Fluorescence-labeled secondary antibodies were diluted in blocking buffer containing 0.5 mg/ml DAPI (Invitrogen), pictures were taken on a confocal microscope (FV1000, Olympus). For paraffin sections, samples were dehydrated through a series of ethanol baths followed by incubation in xylene and embedding in paraffin wax (Paraplast plus, Leica). After sectioning on a rotary microtome (5 μm), sections were deparaffinized and rehydrated followed by hematoxylin/eosin or antibody staining. Hematoxylin staining was performed in Meyer's hemalum solution (Sigma-Aldrich) and eosin staining (Sigma-Aldrich) in H_2O and 50% ethanol. For collagen staining, the sections were incubated in Bounin's solution (Sigma-Aldrich) at 55 °C and stained using 1 g/l aqueous Fast Green FCF (Sigma-Aldrich) solution and 1 g/l Sirius Red F3B (Direct Red 80, Sigma-Aldrich) in saturated aqueous picric acid solution (Sigma-Aldrich). Postnatal heart sections stained with Sirus Red and Fast Green were imaged using a Zeiss AxioScan.Z1 slide scanner. The images were imported to Fiji using the "Bioformats" plugin [44]. Left atria (LA) and the outer left-ventricular walls (LV) were optically dissected and areas containing staining artefacts or physiologically collagen-rich tissues (i.e., cardiac valves and blood vessels) were excluded from the analysis. To segment the tissue from the background, images were filtered for minimum saturation and maximum brightness values in the HSB color space. To assess fibrotic areas within the tissue, filters were complemented with a Hue filter representing red color (185–55 a.u.). The fraction of fibrotic tissue was assessed by normalizing the area of fibrotic tissue on the overall tissue area.

Antibody staining of paraffin sections was performed as described above, including an additional step of peroxidase blocking (1.2% H_2O_2 in PBS, 10 min) and heat-induced antigen retrieval (10 mM sodium citrate buffer, pH 6, 20 min at 85 °C). Primary antibodies: gt anti-Creld1 AF4116 (R&D Systems; 1:250), rb anti-RFP (Rockland; 1:1.000), rb anti-PECAM-1 M20 (Santa Cruz Biotechnology, 1:400), anti-Anp (Peninsula Laboratories, 1:250), anti-Fn1 (Merck, 1:200), anti-Ki67 (Invitrogen, 1:400), anti-cleaved caspase-3 (Asp175, Cell Signaling, 1:400); secondary antibody: dk anti-rat CY3 (Dianova, 1:500).

The Ki67 and cleaved caspase-3 labeling was quantified as follows: Images were taken on a confocal microscope (SP5, Leica). Analysis was performed with Fiji ImageJ (Version 2.0.0-rc-69/1.52p). In brief, random areas of 250 × 250 px were taken from the atria and ventricles, and positive Ki67 cells were manually counted.

Western blot analysis. Lysates were obtained by homogenizing tissue in lysis buffer (10 mM Tris/HCl, pH 7.6, 140 mM NaCl, 1 mM EDTA, 1% Triton X-100, mPIC protease inhibitor cocktail 1:500). Samples were incubated for 30 min on ice and centrifuged at 10,000*g* for 5 min at 4 °C. Prior to separation by SDS-PAGE, samples were mixed with 4× SDS loading-buffer (200 mM Tris/HCl, pH 6.8, 8% SDS (*w/v*), 4% β-mercaptoethanol (*v/v*), 50% glycerol, 0.04% bromophenol blue) and heated for 5 min at 95 °C. Per sample, 80 μg total protein lysates were loaded. For Western blot analysis, proteins were transferred onto PVDF membranes (Immobilon), probed with antibodies following manufacturer's protocols (LI COR IRDye), and analyzed using a near-infrared fluorescence detection system (LI-COR Odyssey). Primary antibodies: gt anti-Creld1 AF4116 (R&D Systems; 1:250), ms anti-tubulin TUB2.1 (Sigma, 1:5.000).

Quantitative real-time PCR. Total RNA was extracted from mouse embryos or mouse hearts using the NucleoSpin XS Kit (Macherey-Nagel) and checked for quality on a 2% agarose gel. 200 ng–2 μg of total RNA were used for cDNA synthesis using SuperScript III Reverse Transcriptase (ThermoFisher Scientific). cDNA was mixed with iQ SYBR Green Supermix (Bio-Rad) or the PowerTrack™ SYBR Green Master Mix (ThermoFisher Scientific) and specific primers to detect relative changes in gene expression. Gene expression was normalized to the expression of reference genes using the delta-Ct method. Primers used for qPCR are described in Table 1.

Cardiovascular examination of endocardial Creld1 knockout mice. $Tie2^{+/cre}$,$Creld1^{flox/flox}$ (15 males, 14 females) and control littermates $Tie2^{+/+}$,$Creld1^{flox/flox}$ (15 males, 15 females) underwent a systematic phenotyping screen by the German Mouse Clinic at the Helmholtz Zentrum München (http://www.mouseclinic.de) as described previously [45–47]. The cardiovascular screening was performed at the age of 15 weeks including electrocardiogram and echocardiography. Briefly, electrocardiography (ECG) measurements were recorded in conscious mice with the ECGenie (Mouse Specificy Inc., Boston, MA) and analyzed using LabChart software (ADInstruments). Left ventricular function was evaluated with transthoracic echocardiography using a Vevo 2100 Imaging System (Visual Sonics) with a 30 MHz probe. No anesthesia was performed for the ECHO measurement.

At 19 weeks of age, hearts were collected, fixed in 4% neutral buffered formalin and embedded in paraffin for histological examination using standard hematoxylin/eosin-stained sections. Heart photomicrographs were taken using a Hamamatsu NanoZoomer digital slide scanner (Hamamatsu Photonics, Herrsching, Germany). Hematoxylin/eosin-stained (H/E) section of the whole heart were imaged using the Zeiss AxioScan.Z1 slice scanner. The images were imported to Fiji using "NDPITools" plugin [48]. Hematoxylin (nuclei) and eosin (cytosolic) staining were separated using the H/E option in the "Color Deconvolution" function integrated into Fiji. The resulting blue (channel 1) and red (channel 2) channels were used to assess nuclei count and tissue area, respectively. Both channels were blurred using a Gaussian blur with $\sigma = 0.55$ μm to suppress noise. Areas with blood clotting, big blood vessels, or noise were excluded from the subsequent analyses. To segment the nuclei, the Fiji auto-thresholding method "RenyiEntropy" was applied. Nuclei objects were identified and counted using the "Analyze Particles" function of Fiji (size range $7.25 * 10^{-12}$ m^2 – $124.2 * 10^{-12}$ m^2, circularity ⩾ 0.25 a.u.). The area of the heart was assessed by counting all pixels passing the threshold obtained by the Fiji auto-thresholding method "Triangle". Cell area was calculated for each image by dividing the count of nuclei by the area covered by the heart.

Sample preparation and RNA sequencing. Total RNA was extracted using a RNeasy Micro kit (Qiagen). The quantity and quality (RINe) of the RNA were assessed via the HS RNA analysis screen tape assay on a 4200 TapeStation system (Agilent Technologies). Total RNA was converted into double-stranded cDNA libraries as a template for high-throughput sequencing according to the SMART-Seq2 protocol [49]. In brief, mRNA was captured by polyT nucleotides and converted into cDNA with 5′ and 3′ overhangs by using the switching mechanism at the 5′ end of RNA template (SMART) approach, SuperScript II RT (Invitrogen) and a template-switching oligonucleotide. After PCR amplification, cDNA was quality controlled via the HS D5000 analysis screen tape assay on a 4200 TapeStation system (Agilent Technologies). A total of 100 pg of cDNA each was further converted to sequencing libraries by Tagmentation using a Tn5 from the Nextera XT DNA Library Preparation kit (Illumina) and subsequent PCR amplification using a Nextera XT Index kit (Illumina). Size selection, purification and size measurement of cDNA fragments were performed as described above. The cDNA library was quantified using a Qubit dsDNA HS assay kit

Table 1
qPCR primer.

Gene	Primer F (5′-3′)	Primer R (5′-3′)
Creld1	GGCCTTGGCTACTTTGAGG	CTACACACTTGAGGTGATGCAG
Nfatc1	TGAGGCTGGTCTTCCGAGTT	CGCTGGGAACACTCTCGATAG
Rcan1	TGCGAGATGGAGGAGGTG	ACTGGAAGGTGGTGTCCTTG
Vegf-a	CACAGCAGATGTGAATGCAG	TTTACACGTCTGCGGATCTT
Hprt	TCCCAGCGTCGTGATTAGCGATGA	AATGTGATGGCCTCCCATCTCCTTCATGACAT
Ppia	GCGTCTCCTTCGAGCTGTT	AAAGTCACCACCCTGGCA
Gapdh	AGGTCGGTGTGAACGGATTTG	TGTAGACCATGTAGTTGAGGTCA
Hprt	TCAGTCAACGGGGGACATAAA	GGGGCTGTACTGCTTAACCAG
Hey1	GCGCGGACGAGAATGGAAA	TCAGGTGATCCACAGTCATCTG
Hey2	AAGCGCCCTTGTGAGGAAAC	GGTAGTTGTCGGTGAATTGGAC
Hes1	CCAGCCAGTGTCAACACGA	AATGCCGGGAGCTATCTTTCT

(Thermo Fisher). The libraries were clustered at 1.4 pM on a NextSeq500 system (Illumina) and sequenced 75-bp single-read using High Output v2 chemistry. Sequencing data were demultiplexed using bcl2fastq2 v.2.20. After base calling and demultiplexing, the 75-bp single-end reads were aligned to the *Mus musculus* reference genome mm10 from UCSC by STAR v.2.5.1 using default parameters.

RNA sequencing analysis. Raw counts were imported to R (R Development Core Team, 2008, v.3.5.3 2019-03-11) and genes with less than 10 reads across all samples were depleted. Subsequently, raw counts were normalized and a differential expression (DE) analysis was conducted using the DESeq2-package [50] set to default parameters. To compensate for unwanted variation, a surrogate variable analysis was performed using the surrogate variable analysis package [51]. The first surrogate variable (SV) was added to the DESeq2-model to obtain more precise dispersion estimates. The regularized logarithm (rlog) transformed counts were additionally corrected on the first SV. The obtained matrix was used as input for the PCA (Rbase package) and gene co-expression network analysis, and to draw heat maps. For the DE analysis, *p*-values were adjusted for the false discovery rate (FDR) using Independent Hypothesis Weighting [52]. PCA results were visualized using the ggplot2 package (v.3.1.1).

For the CoCena[2], raw gene counts were rlog transformed and batch-corrected on the first surrogate variable and subsequently filtered by lowest p-value in any DE comparison (4511 genes total, p-value cutoff 0.055). Gene-to-gene similarities were determined using Spearman's rank correlation coefficient (r) with the R package Hmisc (v.4.2.0) and the threshold to draw edges was set to $r > 0.837$. These cut-off values resulted in networks following the power-law distribution (scale-free topology, $r^2 = 0.86$, Pearson correlation). Unbiased clustering was performed using the "Louvain modularity" algorithm in igraph (v.1.2.4). Clustering was repeated 15 times. Genes assigned to more than five different clusters were not assigned to clusters. Clusters with fewer than 20 genes are not shown. Group fold changes were obtained by calculating the mean of gene-wise z-transformations of the rlog transformed counts in each module. Heatmaps were drawn using the pheatmap package (v.1.0.12). Enrichment analysis was conducted using ClusterProfiler (v.3.10.1) [53]. The results are listed in Supplementary Table S2.

The code for CoCena[2]is available at https://github.com/UlasThomas/CoCena2. The analysis has been performed according to the version from the 25th of March 2019.

The detailed analysis on the embryonic samples was similarly performed using the DEseq2 [50] model correcting for the first sV found the complete dataset [51]. Also in this model, all genes showing a low read count (total reads <10) were removed to de-noise the result. The differential expression was defined according to *p*-values threshold ($p < 0.05$) with no fold change cut-off nor multiple testing correction to identify also small but consistent changes in the transcriptome.

GSEA for the transcriptional profile of KO^{MyHC} E13.5 heart was performed on the ranked gene list according to the log2 fold change in the comparison KO^{MyHC} vs. control. The enrichment and the graphical visualization were calculated with the fgsea R package (v. 1.10.0 https://doi.org/10.1101/060012) with 10000 permutation for statistical testing. All used signatures are part of the MsigDB database (v. 6.2).

Single-cell analysis. Two separate mouse heart single-cell datasets at two different time points (P0, adult) were used to analyze the expression of Creld1 across different cell types. The first dataset was retrieved from the Tabula Muris project [20]. This dataset consisted of processed data of 624 cells of adult mouse aorta-heart tissues using droplet technique (data available from: https://figshare.com/articles/dataset/Robject_files_for_tissues_processed_by_Seurat/5821263?file=13088642). The second dataset consisted of 25,776 processed cells from Drop-seq RNA-seq on a P0 mouse heart (data available from: https://github.com/jlduan/Reprogram-Seq) [19].

Both datasets were separately analyzed in R using Seurat package (v. 3.2.3) [54]. The "NA" cluster from the adult heart dataset and "MEF-derived" cluster from the P0 heart data were excluded from the analysis to focus on cardiac cells only. The remaining cells were visualized using UMAP algorithm and the expression of desired gene(s) in different clusters were shown on the UMAP and dot plots.

Flow cytometry. Pregnant female mice were sacrificed at E13.5 by cervical dislocation. Embryos were removed from the uterus, washed in 4 °C phosphate-buffered saline (PBS, Invitrogen), and dissected hearts were incubated in cold PBS containing 2 mg/ml of collagenase D (Roche), 200 U/ml DNase I (Sigma), and 3% fetal calf serum (FCS, Invitrogen), followed by mechanical disruption and incubation at 37 °C for 30 min. Following the incubation, the cell suspension was filtered through a 100 μm filter, transferred into FACS tubes, and centrifuged at 320*g* for 7 min. Cells were resuspended in FACS buffer (PBS, 0.5% BSA and 2 mM EDTA), containing purified anti-CD16/32 (FccRIII/II) (1:100) and rat serum (2%), and incubated for 10 min at 4 °C. Immunostaining of each sample was performed in two steps. First, each sample was stained with the biotin-labeled antibody Ter119 (1:200, TER-119, Biolegend). Second, the fluorochrome-conjugated antibody mix was applied. Antibodies (Biolegend) used for the second step: CD45 APC-Cy7 (1:400, 30-F11), CD31 PE-Cy7 (1:800, 390), Vcam1 FITC (1:400, 429 (MVCAM.A)), DLL4 APC (1:200, HMD4-1), Notch1 BV421 (1:200, HMN1-12), CD339 (1:100, HMJ1-29), and Streptavidin BV785 (1:200). Each step was performed for 30 min at 4 °C followed by washing cells in FACS buffer and centrifugation at 320*g* for 7 min. Cell suspensions were analyzed by flow cytometry using a BD FACSymphony. Prior to the analysis, Hoechst 33258 was added to the cell suspension (1:10000). Single live cells were gated on the basis of dead cell exclusion, side (SSC-A) and forward scatter (FSC-A) gating, and doublet exclusion using forward scatter width (FSC-W) against FSC-A.

Statistical analysis. Statistical analysis has been performed independent of the sex (female, male) and has been performed in Graph Pad Prism using Student's *t*-test. The respective details are indicated in the figure legends.

For computationally analyzing the flow cytometry data, the open-source statistical software R (version 4.0.2) was used. The samples were down-sampled using the $CD45^-$, $Ter119^-$ gate and batch corrected

using the CytoNorm package version 0.0.5 [55] to reduce technical variances between different experiments. The batch corrected data was loaded using the FlowCore package version 2.0.1 [56]. The aggregated data then was used as the input for further analyses using the CATALYST package (v.1.12.2) [57]. The signal intensities were transformed using the arcsine transformation prior to statistical analysis, with cofactor equal to 150. The transformed data was used for visualization and dimensionality reduction using the Uniform Manifold Approximation and Projection (UMAP) algorithm [58]. Later, the clustering method provided by the CATALYST package was used for an unsupervised grouping of the data. The algorithm is a combination of two methods. The first method applies the FlowSOM clustering [55] that cluster the data points into n x n high-resolution clusters. The second method re-cluster the previously generated clusters into bigger clusters so-called, metaclusters, using the ConsensusClusterPlus metaclustering [59]. The default parameters of the package were used for the processing of data. The appropriate number of metaclusters was chosen by visually inspecting the clusters and their heatmap.

Supplementary data to this article can be found online at https://doi.org/10.1016/j.yjmcc.2021.03.008.

Author contribution

DW, EM, SR, and VB designed the experiments and wrote the manuscript. MK, CK, and DSB performed immunohistochemistry, VB generated the mouse lines and performed mouse phenotyping, SR performed immunohistochemistry and histology, and the RNA-seq analysis together with LB, KH, TU, and ACA. AHK performed and analyzed flow cytometry data together with EM. DW and EM acquired the funding to conduct the experiments. KM performed cardiovascular measurements, KM and NS analyzed data, PSB performed histology of the heart, HF, VGD, and MHdA supervised and coordinated the project at the GMC.

Additional information

The manuscript contains the following Supplementary Information: Table S1, S2, Fig. S1, S2, S3, S4. Schemes were created with BioRender.com

Data availability statement

The data underlying this article are available the GEO repository under GSE159187 at https://www.ncbi.nlm.nih.gov/geo/query/acc.cgi?acc=GSE159187.

Acknowledgement and funding

The work in the labs was supported by the following grants: a) Funded by the Deutsche Forschungsgemeinschaft (DFG, German Research Foundation) under Germany's Excellence Strategy – EXC2151 – 390873048 (to DW and EM) and SPP1926: grant WA3382/2-1 (to DW), SPP1726: grant WA3382/3-1 (to DW), SFB/TRR83 28N (to DW), FOR2743 WA3382/4-1 (to DW), WA3382/1-1 (to DW), GRK 1873/2 (to EM). b) Fritz Thyssen foundation and the Daimler and Benz Foundation (to EM), c) German Federal Ministry of Education and Research: Infrafrontier grant 01KX1012 (to MHdA), German Center for Diabetes Research (DZD) (MHdA). We thank Dr. Bin Zhou (Albert Einstein College of Medicine, Vanderbilt University, USA) for providing Nfatc1-Cre mice, Jens-Henning Krause and Cornelia Cygon for technical support, the Transgenic Service at the LIMES institute (University of Bonn) for their help with the generation of knockout mice, and the Imaging Facility of the Medical Faculty, University of Bonn, for their help with imaging.

Declaration of Competing Interest

The authors declare no competing financial interests.

References

[1] S.W. Robinson, C.D. Morris, E. Goldmuntz, M.D. Reller, M.A. Jones, R.D. Steiner, C. L. Maslen, Missense mutations in CRELD1 are associated with cardiac atrioventricular septal defects, Am. J. Hum. Genet. 72 (4) (2003) 1047–1052.
[2] A. Asim, S. Agarwal, I. Panigrahi, A.N. Sarangi, S. Muthuswamy, A. Kapoor, CRELD1 gene variants and atrioventricular septal defects in Down syndrome, Gene 641 (2018) 180–185.
[3] P. Ghosh, P. Bhaumik, S. Ghosh, U. Ozbek, E. Feingold, C. Maslen, B. Sarkar, V. Pramanik, P. Biswas, B. Bandyopadhyay, S.K. Dey, Polymorphic haplotypes of CRELD1 differentially predispose Down syndrome and euploids individuals to atrioventricular septal defect, Am. J. Med. Genet. A 158A (11) (2012) 2843–2848.
[4] Y. Guo, J. Shen, L. Yuan, F. Li, J. Wang, K. Sun, Novel CRELD1 gene mutations in patients with atrioventricular septal defect, World J. Pediatr. 6 (4) (2010) 348–352.
[5] L. Kusuma, S.M. Dinesh, M.R. Savitha, B. Krishnamurthy, D. Narayanappa, N. B. Ramachandra, A maiden report on CRELD1 single-nucleotide polymorphism association in congenital heart disease patients of Mysore, South India, Genet, Test. Mol. Biomarkers 15 (7–8) (2011) 483–487.
[6] C.L. Maslen, Molecular genetics of atrioventricular septal defects, Curr. Opin. Cardiol. 19 (3) (2004) 205–210.
[7] S. Zhian, J. Belmont, C.L. Maslen, Specific association of missense mutations in CRELD1 with cardiac atrioventricular septal defects in heterotaxy syndrome, Am. J. Med. Genet. A 158A (8) (2012) 2047–2049.
[8] E. Mass, D. Wachten, A.C. Aschenbrenner, A. Voelzmann, M. Hoch, Murine Creld1 controls cardiac development through activation of calcineurin/NFATc1 signaling, Dev. Cell 28 (6) (2014) 711–726.
[9] J.K. Redig, G.T. Fouad, D. Babcock, B. Reshey, E. Feingold, R.H. Reeves, C. L. Maslen, Allelic interaction between CRELD1 and VEGFA in the Pathogenesis of Cardiac Atrioventricular Septal Defects, AIMS Genet. 1 (1) (2014) 1–19.
[10] L.M. Eisenberg, R.R. Markwald, Molecular regulation of atrioventricular valvuloseptal morphogenesis, Circ. Res. 77 (1) (1995) 1–6.
[11] S.M. Savolainen, J.F. Foley, S.A. Elmore, Histology atlas of the developing mouse heart with emphasis on E11.5 to E18.5, Toxicol. Pathol. 37 (4) (2009) 395–414.
[12] A.F. Moorman, V.M. Christoffels, Cardiac chamber formation: development, genes, and evolution, Physiol. Rev. 83 (4) (2003) 1223–1267.
[13] L.A. Samsa, B. Yang, J. Liu, Embryonic cardiac chamber maturation: trabeculation, conduction, and cardiomyocyte proliferation, Am. J. Med. Genet. C: Semin. Med. Genet. 163C (3) (2013) 157–168.
[14] J. Grego-Bessa, L. Luna-Zurita, G. del Monte, V. Bolos, P. Melgar, A. Arandilla, A. N. Garratt, H. Zang, Y.S. Mukouyama, H. Chen, W. Shou, E. Ballestar, M. Esteller, A. Rojas, J.M. Perez-Pomares, J.L. de la Pompa, Notch signaling is essential for ventricular chamber development, Dev. Cell 12 (3) (2007) 415–429.
[15] G. D'Amato, G. Luxan, G. del Monte-Nieto, B. Martinez-Poveda, C. Torroja, W. Walter, M.S. Bochter, R. Benedito, S. Cole, F. Martinez, A.K. Hadjantonakis, A. Uemura, L.J. Jimenez-Borreguero, J.L. de la Pompa, Sequential Notch activation regulates ventricular chamber development, Nat. Cell Biol. 18 (1) (2016) 7–20.
[16] G. Luxan, J.C. Casanova, B. Martinez-Poveda, B. Prados, G. D'Amato, D. MacGrogan, A. Gonzalez-Rajal, D. Dobarro, C. Torroja, F. Martinez, J. L. Izquierdo-Garcia, L. Fernandez-Friera, M. Sabater-Molina, Y.Y. Kong, G. Pizarro, B. Ibanez, C. Medrano, P. Garcia-Pavia, J.R. Gimeno, L. Monserrat, L.J. Jimenez-Borreguero, J.L. de la Pompa, Mutations in the NOTCH pathway regulator MIB1 cause left ventricular noncompaction cardiomyopathy, Nat. Med. 19 (2) (2013) 193–201.
[17] G. Del Monte-Nieto, M. Ramialison, A.A.S. Adam, B. Wu, A. Aharonov, G. D'Uva, L. M. Bourke, M.E. Pitulescu, H. Chen, J.L. de la Pompa, W. Shou, R.H. Adams, S. K. Harten, E. Tzahor, B. Zhou, R.P. Harvey, Control of cardiac jelly dynamics by NOTCH1 and NRG1 defines the building plan for trabeculation, Nature 557 (7705) (2018) 439–445.
[18] L. Bonaguro, M. Kohne, L. Schmidleithner, J. Schulte-Schrepping, S. Warnat-Herresthal, A. Horne, P. Kern, P. Gunther, R. Ter Horst, M. Jaeger, S. Rahmouni, M. Georges, C.S. Falk, Y. Li, E. Mass, M. Beyer, L.A.B. Joosten, M.G. Netea, T. Ulas, J.L. Schultze, A.C. Aschenbrenner, CRELD1 modulates homeostasis of the immune system in mice and humans, Nat. Immunol. 21 (12) (2020) 1517–1527.
[19] J. Duan, B. Li, M. Bhakta, S. Xie, P. Zhou, N.V. Munshi, G.C. Hon, Rational reprogramming of cellular states by combinatorial perturbation, Cell Rep. 27 (12) (2019) 3486–3499 e6.
[20] Tabula Muris Consortium, Overall coordination, Logistical coordination, Organ collection and processing, Library preparation and sequencing, Computational data analysis, Cell type annotation, Writing group, Supplemental text writing group, Principal investigators, Single-cell transcriptomics of 20 mouse organs creates a Tabula Muris, Nature 562 (7727) (2018) 367–372.
[21] F. Schwenk, U. Baron, K. Rajewsky, A cre-transgenic mouse strain for the ubiquitous deletion of loxP-flanked gene segments including deletion in germ cells, Nucleic Acids Res. 23 (24) (1995) 5080–5081.
[22] A.C. Aschenbrenner, M. Mouktaroudi, B. Kraemer, N. Antonakos, M. Oestreich, K. Gkizeli, M. Nuesch-Germano, M. Saridaki, L. Bonaguro, N. Reusch, K. Bassler, S. Doulou, R. Knoll, T. Pecht, T.S. Kapellos, N. Rovina, C. Kroeger, M. Herbert, L. Holsten, A. Horne, I.D. Gemuend, S. Agrawal, K. Dahm, M. van Uelft, A. Drews, L. Lenkeit, N. Bruse, J. Gerretsen, J. Gierlich, M. Becker, K. Haendler, M. Kraut,

H. Theis, S. Mengiste, E. De Domenico, J. Schulte-Schrepping, L. Seep, J. Raabe, C. Hoffmeister, M. ToVinh, V. Keitel, G.J. Rieke, V. Talevi, A.N. Aziz, P. Pickkers, F. van de Veerdonk, M.G. Netea, J.L. Schultze, M. Kox, M.M.B. Breteler, J. Nattermann, A. Koutsoukou, E.J. Giamarellos-Bourboulis, T. Ulas, Disease severity-specific neutrophil signatures in blood transcriptomes stratify COVID-19 patients, medRxiv (2020). PMID: 33441124.

[23] G. Kessler-Icekson, Y. Barhum, J. Schaper, W. Schaper, E. Kaganovsky, T. Brand, ANP expression in the hypertensive heart, Exp. Clin. Cardiol. 7 (2–3) (2002) 80–84.

[24] K.P. Hanson, J.P. Jung, Q.A. Tran, S.P. Hsu, R. Iida, V. Ajeti, P.J. Campagnola, K. W. Eliceiri, J.M. Squirrell, G.E. Lyons, B.M. Ogle, Spatial and temporal analysis of extracellular matrix proteins in the developing murine heart: a blueprint for regeneration, Tissue Eng. Part. A 19 (9–10) (2013) 1132–1143.

[25] T.D. Camenisch, A.P. Spicer, T. Brehm-Gibson, J. Biesterfeldt, M.L. Augustine, A. Calabro Jr., S. Kubalak, S.E. Klewer, J.A. McDonald, Disruption of hyaluronan synthase-2 abrogates normal cardiac morphogenesis and hyaluronan-mediated transformation of epithelium to mesenchyme, J. Clin. Invest. 106 (3) (2000) 349–360.

[26] S. Hatano, K. Kimata, N. Hiraiwa, M. Kusakabe, Z. Isogai, E. Adachi, T. Shinomura, H. Watanabe, Versican/PG-M is essential for ventricular septal formation subsequent to cardiac atrioventricular cushion development, Glycobiology 22 (9) (2012) 1268–1277.

[27] R. Kopan, M.X. Ilagan, The canonical Notch signaling pathway: unfolding the activation mechanism, Cell 137 (2) (2009) 216–233.

[28] K. Oh-hashi, R. Kunieda, Y. Hirata, K. Kiuchi, Biosynthesis and secretion of mouse cysteine-rich with EGF-like domains 2, FEBS Lett. 585 (15) (2011) 2481–2487.

[29] S.T. Boyle, V. Poltavets, J. Kular, N.T. Pyne, J.J. Sandow, A.C. Lewis, K.J. Murphy, N. Kolesnikoff, P.A.B. Moretti, M.N. Tea, V. Tergaonkar, P. Timpson, S.M. Pitson, A.I. Webb, R.J. Whitfield, A.F. Lopez, M. Kochetkova, M.S. Samuel, ROCK-mediated selective activation of PERK signalling causes fibroblast reprogramming and tumour progression through a CRELD2-dependent mechanism, Nat. Cell Biol. 22 (7) (2020) 882–895.

[30] K. Kuwahara, T. Nishikimi, K. Nakao, Transcriptional regulation of the fetal cardiac gene program, J. Pharmacol. Sci. 119 (3) (2012) 198–203.

[31] A.H. Li, P.P. Liu, F.J. Villarreal, R.A. Garcia, Dynamic changes in myocardial matrix and relevance to disease: translational perspectives, Circ. Res. 114 (5) (2014) 916–927.

[32] M.H. Konstandin, M. Volkers, B. Collins, P. Quijada, M. Quintana, A. De La Torre, L. Ormachea, S. Din, N. Gude, H. Toko, M.A. Sussman, Fibronectin contributes to pathological cardiac hypertrophy but not physiological growth, Basic Res. Cardiol. 108 (5) (2013) 375.

[33] H. Li, S. Cherry, D. Klinedinst, V. DeLeon, J. Redig, B. Reshey, M.T. Chin, S. L. Sherman, C.L. Maslen, R.H. Reeves, Genetic modifiers predisposing to congenital heart disease in the sensitized Down syndrome population, Circ. Cardiovasc. Genet. 5 (3) (2012) 301–308.

[34] M. D'Alessandro, M. Richard, C. Stigloher, V. Gache, T. Boulin, J.E. Richmond, J. L. Bessereau, CRELD1 is an evolutionarily-conserved maturational enhancer of ionotropic acetylcholine receptors, Elife 7 (2018).

[35] V. Baladron, M.J. Ruiz-Hidalgo, M.L. Nueda, M.J. Diaz-Guerra, J.J. Garcia-Ramirez, E. Bonvini, E. Gubina, J. Laborda, dlk acts as a negative regulator of Notch1 activation through interactions with specific EGF-like repeats, Exp. Cell Res. 303 (2) (2005) 343–359.

[36] Z. Cao, R. Lis, M. Ginsberg, D. Chavez, K. Shido, S.Y. Rabbany, G.H. Fong, T. P. Sakmar, S. Rafii, B.S. Ding, Targeting of the pulmonary capillary vascular niche promotes lung alveolar repair and ameliorates fibrosis, Nat. Med. 22 (2) (2016) 154–162.

[37] V. Rodilla, A. Villanueva, A. Obrador-Hevia, A. Robert-Moreno, V. Fernandez-Majada, A. Grilli, N. Lopez-Bigas, N. Bellora, M.M. Alba, F. Torres, M. Dunach, X. Sanjuan, S. Gonzalez, T. Gridley, G. Capella, A. Bigas, L. Espinosa, Jagged1 is the pathological link between Wnt and Notch pathways in colorectal cancer, Proc. Natl. Acad. Sci. U. S. A. 106 (15) (2009) 6315–6320.

[38] S. Estrach, C.A. Ambler, C. Lo Celso, K. Hozumi, F.M. Watt, Jagged 1 is a beta-catenin target gene required for ectopic hair follicle formation in adult epidermis, Development 133 (22) (2006) 4427–4438.

[39] C.I. Rodriguez, F. Buchholz, J. Galloway, R. Sequerra, J. Kasper, R. Ayala, A. F. Stewart, S.M. Dymecki, High-efficiency deleter mice show that FLPe is an alternative to Cre-loxP, Nat. Genet. 25 (2) (2000) 139–140.

[40] P.A. Koni, S.K. Joshi, U.A. Temann, D. Olson, L. Burkly, R.A. Flavell, Conditional vascular cell adhesion molecule 1 deletion in mice: impaired lymphocyte migration to bone marrow, J. Exp. Med. 193 (6) (2001) 741–754.

[41] B. Wu, Z. Zhang, W. Lui, X. Chen, Y. Wang, A.A. Chamberlain, R.A. Moreno-Rodriguez, R.R. Markwald, B.P. O'Rourke, D.J. Sharp, D. Zheng, J. Lenz, H. S. Baldwin, C.P. Chang, B. Zhou, Endocardial cells form the coronary arteries by angiogenesis through myocardial-endocardial VEGF signaling, Cell 151 (5) (2012) 1083–1096.

[42] R. Agah, P.A. Frenkel, B.A. French, L.H. Michael, P.A. Overbeek, M.D. Schneider, Gene recombination in postmitotic cells. Targeted expression of Cre recombinase provokes cardiac-restricted, site-specific rearrangement in adult ventricular muscle in vivo, J. Clin. Invest. 100 (1) (1997) 169–179.

[43] L. Madisen, T.A. Zwingman, S.M. Sunkin, S.W. Oh, H.A. Zariwala, H. Gu, L.L. Ng, R.D. Palmiter, M.J. Hawrylycz, A.R. Jones, E.S. Lein, H. Zeng, A robust and high-throughput Cre reporting and characterization system for the whole mouse brain, Nat. Neurosci. 13 (1) (2010) 133–140.

[44] M. Linkert, C.T. Rueden, C. Allan, J.M. Burel, W. Moore, A. Patterson, B. Loranger, J. Moore, C. Neves, D. Macdonald, A. Tarkowska, C. Sticco, E. Hill, M. Rossner, K. W. Eliceiri, J.R. Swedlow, Metadata matters: access to image data in the real world, J. Cell Biol. 189 (5) (2010) 777–782.

[45] V. Gailus-Durner, H. Fuchs, L. Becker, I. Bolle, M. Brielmeier, J. Calzada-Wack, R. Elvert, N. Ehrhardt, C. Dalke, T.J. Franz, E. Grundner-Culemann, S. Hammelbacher, S.M. Holter, G. Holzlwimmer, M. Horsch, A. Javaheri, S. V. Kalaydjiev, M. Klempt, E. Kling, S. Kunder, C. Lengger, T. Lisse, T. Mijalski, B. Naton, V. Pedersen, C. Prehn, G. Przemeck, I. Racz, C. Reinhard, P. Reitmeir, I. Schneider, A. Schrewe, R. Steinkamp, C. Zybill, J. Adamski, J. Beckers, H. Behrendt, J. Favor, J. Graw, G. Heldmaier, H. Hofler, B. Ivandic, H. Katus, P. Kirchhof, M. Klingenspor, T. Klopstock, A. Lengeling, W. Muller, F. Ohl, M. Ollert, L. Quintanilla-Martinez, J. Schmidt, H. Schulz, E. Wolf, W. Wurst, A. Zimmer, D.H. Busch, M.H. de Angelis, Introducing the German Mouse Clinic: open access platform for standardized phenotyping, Nat. Methods 2 (6) (2005) 403–l.

[46] H. Fuchs, J.A. Aguilar-Pimentel, O.V. Amarie, L. Becker, J. Calzada-Wack, Y.L. Cho, L. Garrett, S.M. Holter, M. Irmler, M. Kistler, M. Kraiger, P. Mayer-Kuckuk, K. Moreth, B. Rathkolb, J. Rozman, P. da Silva Buttkus, I. Treise, A. Zimprich, K. Gampe, C. Hutterer, C. Stoger, S. Leuchtenberger, H. Maier, M. Miller, A. Scheideler, M. Wu, J. Beckers, R. Bekeredjian, M. Brielmeier, D.H. Busch, M. Klingenspor, T. Klopstock, M. Ollert, C. Schmidt-Weber, T. Stoger, E. Wolf, W. Wurst, A.O. Yildirim, A. Zimmer, V. Gailus-Durner, M. Hrabe de Angelis, Understanding gene functions and disease mechanisms: phenotyping pipelines in the German Mouse Clinic, Behav. Brain Res. 352 (2018) 187–196.

[47] H. Fuchs, V. Gailus-Durner, T. Adler, J.A. Aguilar-Pimentel, L. Becker, J. Calzada-Wack, P. Da Silva-Buttkus, F. Neff, A. Gotz, W. Hans, S.M. Holter, M. Horsch, G. Kastenmuller, E. Kemter, C. Lengger, H. Maier, M. Matloka, G. Moller, B. Naton, C. Prehn, O. Puk, I. Racz, B. Rathkolb, W. Romisch-Margl, J. Rozman, R. Wang-Sattler, A. Schrewe, C. Stoger, M. Tost, J. Adamski, B. Aigner, J. Beckers, H. Behrendt, D.H. Busch, I. Esposito, J. Graw, T. Illig, B. Ivandic, M. Klingenspor, T. Klopstock, E. Kremmer, M. Mempel, S. Neschen, M. Ollert, H. Schulz, K. Suhre, E. Wolf, W. Wurst, A. Zimmer, M. Hrabe de Angelis, Mouse phenotyping, Methods 53 (2) (2011) 120–135.

[48] C. Deroulers, D. Ameisen, M. Badoual, C. Gerin, A. Granier, M. Lartaud, Analyzing huge pathology images with open source software, Diagn. Pathol. 8 (2013) 92.

[49] S. Picelli, O.R. Faridani, A.K. Bjorklund, G. Winberg, S. Sagasser, R. Sandberg, Full-length RNA-seq from single cells using Smart-seq2, Nat. Protoc. 9 (1) (2014) 171–181.

[50] M.I. Love, W. Huber, S. Anders, Moderated estimation of fold change and dispersion for RNA-seq data with DESeq2, Genome Biol. 15 (12) (2014) 550.

[51] J.T. Leek, W.E. Johnson, H.S. Parker, A.E. Jaffe, J.D. Storey, The sva package for removing batch effects and other unwanted variation in high-throughput experiments, Bioinformatics 28 (6) (2012) 882–883.

[52] N. Ignatiadis, B. Klaus, J.B. Zaugg, W. Huber, Data-driven hypothesis weighting increases detection power in genome-scale multiple testing, Nat. Methods 13 (7) (2016) 577–580.

[53] G. Yu, L.G. Wang, Y. Han, Q.Y. He, clusterProfiler: an R package for comparing biological themes among gene clusters, OMICS 16 (5) (2012) 284–287.

[54] R. Satija, J.A. Farrell, D. Gennert, A.F. Schier, A. Regev, Spatial reconstruction of single-cell gene expression data, Nat. Biotechnol. 33 (5) (2015) 495–502.

[55] S. Van Gassen, B. Gaudilliere, M.S. Angst, Y. Saeys, N. Aghaeepour, CytoNorm: a normalization algorithm for cytometry data, Cytometry A 97 (3) (2020) 268–278.

[56] B. Ellis, P. Haaland, F. Hahne, N. Le Meur, N. Gopalakrishan, J. Spidlen, M. Jiang, G. Finak, S. Granjeaud, FlowCore: flowCore: Basic Structures for Flow Cytometry Data, R package version 2.0.1, 2020.

[57] H.L. Crowell, V.R.T. Zantonelli, S. Chevrier, M.D. Robinson, B. Bodenmiller, Cytometry dATa anALYSis Tools, R package version 1.12.2, 2020.

[58] L. McInnes, J. Healy, J. Melville, UMAP: Uniform Manifold Approximation and Projection for dimension reduction, J. Open Source Softw. 3 (29) (2018) 861, https://doi.org/10.21105/joss.00861.

[59] M.D. Wilkerson, D.N. Hayes, ConsensusClusterPlus: a class discovery tool with confidence assessments and item tracking, Bioinformatics 26 (12) (2010) 1572–1573.